

A Promise of Realizable, Ultra-Scalable Communications at nano-Scale: A multi-Modal nano-Machine Architecture

Christos Liaskos and Angeliki Tsioliariidou

Abstract—Wireless networks of nano-nodes will play a critical role in future medical, quality control, environmental monitoring and military applications. Nano-nodes are invisible/marginally visible to the human eye, ranging in size from approximately $100\mu m$ to few nanometers. Nano-networking poses unique challenges, requiring ground-breaking solutions. Firstly, the nano-scale imposes severe restrictions to the computational and communication capabilities of the nodes. Secondly, nano-nodes are not accessible for programming, configuration and debugging in the classical sense. Thus, a nano-network should be self-configuring, resilient and adaptive to environmental changes. Finally, all nano-networking protocols should be ultra-scalable, since a typical nano-network may comprise billions of nodes. The study contributes a novel paradigm for data dissemination in networking nano-machines, addressing these unique challenges. Relying on innovative analytical results on lattice algebra and nature-inspired processes, a novel data dissemination method is proposed. The nano-nodes exploit their environmental feedback and mature adaptively into network backbone or remain single network users. Such a process can be implemented as an ultra-scalable, low complexity, multi-modal nano-node architecture (physical layer), providing efficient networking and application services at the same time. Requiring existing manufacturing technology, the proposed architecture constitutes the first candidate solution for realizable nano-networking.

Index Terms—Wireless Networking, Nanoscale.

1 INTRODUCTION

NANO-NETWORKS will expand the reach of the Web and automated control at the levels of cells and molecules. Automated drug delivery and tumor cell detection in medicine, air, water and generic material quality control in the industry and environmental monitoring are but a few of the envisioned applications of nano-networks. The networking of nano-machines poses unique challenges that require radically new solutions [1]. Firstly, a nano-machine is severely restricted in computational power and memory. Power restrictions add

up to this limitation as well. Secondly, a nano-network is vast, even when compared to the Web. Comprising billions of nodes, nano-networking requires ultra-scalable communication protocols and low-cost design per node. Finally, the nano-scale implies that a nano-node is inaccessible for programming, debugging and configuration in the classical sense. Thus, a nano-network should be self-organizing and self-maintained. The study of a realistically complex nano-node architecture that combines these attributes is the goal of the present paper. We present a viable nano-node architecture for 2D, static topologies which can be implemented at present on silicon wafers.

A nano-node is a compact but complete computing unit, comprising a power supply, a memory and a CPU module. Networking nano-nodes also requires a communications module. Finally, a sensory module or an actuator can act as the node's connection to its environment. Ongoing research on each separate node part has reached notable levels. Power supply modules are the most challenging to implement. Standalone batteries at mm^2 size can yield a capacity of $2.75\mu Ah$ at $2.5\mu A$ discharge [2]. However, viable alternatives, such as external, inductive power supplies, can offer similar performance. CPU and memory modules are tractable to implement, given that mainstream CPUs are constructed with nm transistor spacing. Thus, a set of logical gates or operational amplifiers are implementable on a $100nm^2$ surface, able to perform simple operations. Additionally, chemical sensors can be constructed at $100nm$ since 2000 [3], based on carbon nano-tubes. Regarding communication, two classes of modules are defined. Molecular communication assumes the ability to manipulate molecules, such as hormones, imbuing them with information and diffusing them to a given environment [4]. Alternatively, a currently realizable class, which is adopted in the present study, is the miniature version of the classic RF modules [5]–[7], which can be shrunk to $800 \times 600nm$ [1], including the antenna, the tuner, the amplifier and the modulator/demodulator units. Ongoing research is expected to reduce the aggregate size of a nano-node to a few hundred nm^2 in the near future [8].

With approximately 1000 transistors per nano-node to accommodate all computing and data storage capabili-

C. Liaskos is with the Telecommunications and Networks Laboratory, Institute of Computer Science, Foundation of Research and Technology, Hellas (FORTH), P.O. Box 1385, GR-711 10, Heraklion, Crete, Greece, e-mail: cliaskos@ics.forth.gr.

A. Tsioliariidou is with the Department of Electrical and Computer Engineering, Democritus University of Thrace, 67100, Xanthi, Greece, email: atsiolia@ee.duth.gr

The authors would like to thank prof. Andreas Pitsillides (University of Cyprus, Andreas.Pitsillides@ucy.ac.cy) and Nikolaos Kantartzis (Aristotle University, Greece, kant@ee.auth.gr) for their valuable insights and continued support of the present study.

ties, a TCP-based, or similar, nano-networking protocol stack is out of the question [1]. The TCP and OSI models assume fully programmable, general purpose computing machinery with considerable processing power and an adequate power supply. Then, dividing the communication process to Physical (PHY), Medium Access (MAC), Networking (NET) and Application (APP) layers allowed for specialized research and modular operation of the proposed algorithms, albeit increasing the overall overhead and complexity. In stark contrast, nano-nodes are inconfigurable and custom-made for each application scenario. Furthermore, there is no layer discrimination, as imposed by the computing and power limitations. A single layer (PHY) must combine all needed MAC, NET, APP and even security capabilities in an interleaved manner [9], while keeping the overall complexity and power consumption within the restrictions of the scale. Upholding these conditions, we present an adaptive, energy-efficient, self-configuring networking architecture for 2D nano-networks. It combines MAC, NET and APP functionalities in one multimodal, low complexity layer. Furthermore, novel analytical results prove the architecture to be ultra-scalable, operating efficiently regardless of the total number of nodes. Apart from introducing the first complete nano-networking paradigm, the proposed architecture is readily implementable with existing silicon wafer carving technologies, typically employed in mainstream CPU manufacturing.

The remainder of this paper is organized as follows. Related studies are reviewed in Section 2. Sections 3 and 4 analytically study the interference patterns of sparse and dense nano-networks. The node maturity process is described in Section 6. Simulation results are given in Section 7. The conclusion follows in Section 8.

2 RELATED WORK

Related studies in nano-communications have so far dealt with wireless channel modeling (PHY) and MAC-layer issues.

Electromagnetic nano-communication, which is assumed in the present study operates at the THz spectrum and employs graphene-based antennas [10]. The propagation speed of electromagnetic waves in carbon nanotubes and patches can be up to two orders of magnitude lower than in traditional materials. This phenomenon enables the miniaturization of the antennas at nano-scale, while keeping the operating frequency tractably high (THz) [1]. Under these conditions, the physics of electromagnetic propagation are not affected by quantum phenomena. Thus, the employed channel model is the classic one used in macro-scale wireless communications. Change is encountered only at the wave attenuation models, assuming that the nano-network is submerged into a chemical solution. Otherwise, the classic free space loss model is used [10].

Jornet et al. proposed a statistical THz-wireless channel model for nanomachines dispersed in gas mixtures in

[10]. Node communication is discussed at a higher level in [6], [11]. The study considers the Rate Division Time Spread On-Off Keying (RD TS-OOK) as a prominent modulation scheme. Each node uses short bursts to represent logical "1" and silence for zeros. The burst duration is much smaller than the symbol duration, while each node uses random inter-bit intervals and burst amplitudes. Thus, collisions are minimized in a probabilistic manner. A lightweight, handshake-based MAC protocol (PHLAME) is then proposed on top of RD TS-OOK. Arguing that this style of point-to-point communication may not be appropriate for the severely restricted nano-environment, Srinath et al. proposed the clustering of nano-nodes into groups, delegating communication abilities only to their more-powerful cluster masters [7]. The nano-nodes should still support an addressing protocol, a timing system for duty-cycle operation, and a few powerful cluster heads dispersed throughout the covered area.

Powerful nano-machines with complex communication capabilities may emerge in the far future. Nonetheless, efficient communication protocols that do not require such complexity would be more practical. Notice that nano-machines should not only be implementable, but also cheap, since a typical network may comprise several millions to billions of them. In this aspect, it is worth mentioning lightweight solutions targeting classic macro-scale networks. Flooding is a technique aiming at disseminating data throughout a network by blind retransmission [12]. Nonetheless, it incurs a high rate of redundant packets, a problem known as the "broadcast storm" [13]. To mitigate for this issue, a node may re-transmit a message probabilistically [14]. The retransmission probability requires optimization, which is accomplished by data exchange between nodes. For example, in [15] the nodes share their movement patterns, approximating their local distribution over time. A similar approach is followed in [16], which adopts an additional MAC protocol to limit the interferences further. Shen et. al proposed the use of directional antennas to limit interference and redundant transmissions. The directions of the antennas are set according to the bond percolation of the node graph [17]. Phase-transition phenomena may also be exploited, as in [18], but require extensive experimentation to assess applicability and parameterization. In general, probabilistic flood reduces redundant broadcasts, but increases complexity due to the need for optimization-related data exchange between the nodes.

The present study differentiates by contributing a realizability-oriented, lightweight and efficient nano-networking architecture. Without requiring any node addressing and node neighborhood information, it defines the following workflow. Once a node obtains a useful measurement from its sensory module it becomes a source, emitting pulses ("packets") periodically in a push-based manner. Receiving nodes adopt a flooding scheme, initially retransmitting the packet uncondition-

ally. During this environmental sounding, called “node maturity process”, each node processes statistically its Signal-to-Interference (SINR) levels and subsequently matures to become either networking “infrastructure” (re-transmitter) or network “user”. Users can exemplarily doze, enter ready-only mode or continue their sensing duties. The process is adaptive, with the nodes turning into users or infrastructure according to the existing resources. Using novel analytical methods of point lattice algebra, the study proved that this networking paradigm is infinitely scalable, operating efficiently regardless of the number of nodes. Furthermore, extensive simulations show that: (1) A high number of nodes can be turned off (users), especially in dense networks, promoting energy efficiency. (2) Information is propagated optimally through the network, while requiring much fewer total transmissions than alternative approaches. (3) The “infrastructure” nodes form well-formed, symmetrical patterns, such as stars and snowflakes. This property can be used for pinpointing the packet source location with good accuracy, without any timestamps or additional mechanisms. Finally, the symmetry can be used for directing the packet transmissions towards specific directions, achieving the same effects as beamforming or directional routing.

3 SYMMETRY AND NODE PATTERNS IN GRID LAYOUTS

Assume a set of nodes arranged on the vertexes of a square grid of indefinite size, as depicted in Fig. 1. The reader is encouraged to visualize each node as a trivial, autonomous circuit, which is offset indefinitely on a silicon wafer. Each node is equipped with a patch antenna providing a circular connectivity pattern [19]. For this Section of the analysis, it is assumed that a node has its eight immediate neighbors within its range, as shown by the arrows surrounding the source at the axes origin. The size of a grid cell is at the $nm-\mu m$ scale. A packet flood is triggered by the source. Any node that receives a packet from a neighbor re-broadcasts it immediately, provided that it has received it for the first time. We are interested in pinpointing the nodes which experience the highest electromagnetic interference while receiving a packet.

The study assumes a standard interference model based on SINR (Signal-to-Interference Ratios). The most prominent modulation scheme for wireless nano-communications is the direct representation of a logical “1” as a very short pulse, while silence stands for a “0” [5]. In addition, the duration of the “1”-pulse is at the scale of $T_p = 0.1nsec$. The interval between two consecutive bits is $T_b \gg T_p$. A non-coherent receiver integrates incoming pulses over $T_i = 10 \cdot T_p$ time intervals [6]. Consequently, bitstreams that arrive to a receiver

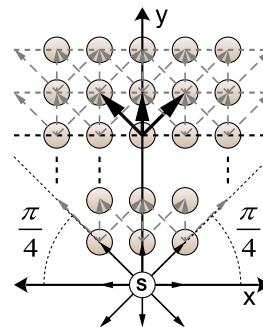


Figure 1: Propagation of messages via flood-based dissemination in a grid arrangement of nodes. Each node has its eight immediate neighbors within its range. The source “s” is placed at the axes origin.

can collide¹. Therefore, the ratio of the power of the useful signal to the interference and noise combination is assumed to be the determinant factor of successful packet receptions.

Making use of the symmetry in node connections, we divide the plane in four sectors defined by the lines $\theta = \pi/4$, $\theta = 3\pi/4$. The phenomena inside and on the borders of these sectors will be studied separately.

Inside the sector depicted in Fig. 1 the synchronously informed nodes form lines perpendicular to the y -axis (strong dashed lines). This kind of advancing front formation is due to the form of the node connections. A new front line is produced by the preceding one. Notice that the node connections parallel to the front do not contribute to this process, since they affect already informed nodes. Thus, a packet propagates in the sector through the three directions denoted in bold.

With no loss of generality, assume that the grid cells have unary-sized sides. A packet may arrive to a node at coordinates (x, y) through any linear combination of the three dominant directions, forming the following Diophantine system:

$$\begin{bmatrix} x \\ y \end{bmatrix} = n_1 \begin{bmatrix} 1 \\ 1 \end{bmatrix} + n_2 \begin{bmatrix} -1 \\ 1 \end{bmatrix} + n_3 \begin{bmatrix} 0 \\ 1 \end{bmatrix}, \quad n_1, n_2, n_3 \in \mathbb{N} \quad (1)$$

Notice that the tuple $\langle n_1, n_2, n_3 \rangle$ defines the length \mathbb{S} of a given path, regardless of the ordering of the hops:

$$\mathbb{S} = (n_1 + n_2) \cdot \sqrt{2} + n_3 \cdot 1 \quad (2)$$

Equations (1) and (2) can be treated as a fully-defined, 3×3 linear system which is solved for n_1, n_2, n_3 as follows:

$$n_1 = \frac{x + y}{2} + \frac{\mathbb{S} - \sqrt{2}y}{2(\sqrt{2} - 1)} \quad (3)$$

$$n_2 = \frac{y - x}{2} + \frac{\mathbb{S} - \sqrt{2}y}{2(\sqrt{2} - 1)} \quad (4)$$

1. Notice that the “pulses” themselves may not often collide, due to their short duration, but the packets, i.e. the series of bits can, especially after the integration at the receiver. For the same reason, identical packets (i.e. waveforms) that arrive at a node with small delay can also contribute constructively.

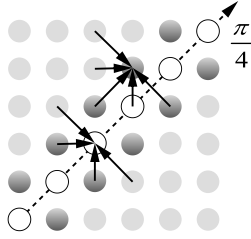


Figure 2: Study of the packet collision events on the $\theta = \pi/4, 3\pi/4$ symmetry lines of Fig. 1. Nodes adjacent to the lines (darker color) suffer the most interference. Grayed circles represent the nodes that have already received the propagating message due to the straightforward propagation of Fig. 1.

$$n_3 = \frac{-\mathbb{S} + \sqrt{2}y}{\sqrt{2} - 1} \quad (5)$$

The quantities n_1, n_2, n_3 represent positive integers, introducing the following restrictions:

- $n_1 \geq 0 \iff y - (\sqrt{2} - 1) \cdot x \leq \mathbb{S}$
- $n_2 \geq 0 \iff y + (\sqrt{2} - 1) \cdot x \leq \mathbb{S}$
- $n_3 \geq 0 \iff \mathbb{S} \leq \sqrt{2}y$

Concerning the first two inequalities, it holds that:

- $x \geq 0 \iff y - (\sqrt{2} - 1) \cdot x \leq y + (\sqrt{2} - 1) \cdot x$
- $x \leq 0 \iff y + (\sqrt{2} - 1) \cdot x \leq y - (\sqrt{2} - 1) \cdot x$

Therefore, the first two restrictions on \mathbb{S} are:

$$y + |x| \cdot (\sqrt{2} - 1) \leq \mathbb{S} \quad (6)$$

Furthermore, it holds that:

$$y + |x| \cdot (\sqrt{2} - 1) \leq \sqrt{2}y \iff |x| \leq y \quad (7)$$

which is true, since we examine the area defined by the angles $\pi/4 \leq \theta \leq 3\pi/4$. Thus, the value set of \mathbb{S} is:

$$y + |x| \cdot (\sqrt{2} - 1) \leq \mathbb{S} \leq \sqrt{2}y \quad (8)$$

The width of the value set,

$$W(x, y) = (y - |x|) \cdot (\sqrt{2} - 1) \quad (9)$$

expresses the number of different propagation paths (length-wise) arriving to a point (x, y) from a source located at the axes origin. A wider value set means that more echoes arrive at the given (x, y) point, inferring a higher amount of interference and lower signal reception quality. Furthermore, equation (9) is maximized on the line $x = 0$. Taking the quadrant symmetry into account we deduce:

Lemma 1. *Assume flood-based packet propagation on a square grid topology, where each node has its eight immediate neighbors within its range. The nodes on the lines $x = 0$ and $y = 0$ with regard to the source of the original packet experience the highest interference.*

We proceed to study the phenomena on the symmetry lines $\theta = \pi/4, 3\pi/4$, where the propagation fronts of two adjacent quadrants collide. A detail of the phenomenon

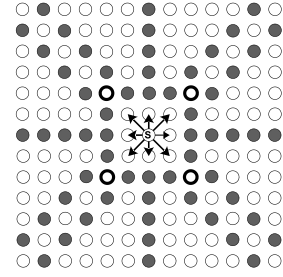


Figure 3: The expected pattern of nodes experiencing high interference. The connectivity pattern of the nodes is denoted by the black arrows originating from the source “s”. Notice that the nodes in bold act as gateways to their respective quadrants. Switching them on or off properly can have the effects of data routing (direction-selective dissemination).

is given in Fig. 2. Notice that due to the node connectivity pattern, the fronts interact only with the nodes on $\theta = \pi/4$ and on the adjacent lines. Furthermore, the two fronts affect the white-colored nodes on $\theta = \pi/4$ in a symmetrical manner. In other words, any path of the upper quadrant leading to a white-colored node has a corresponding, equally-sized, non-interfering path in the lower quadrant. Thus, the $W(x, y)$ values, representing width of value sets, are not affected. On the other hand, this symmetry is upset at the nodes adjacent to the $\theta = \pi/4$ line, leading to higher expected interference.

Conclusively, the expected positions of nodes experiencing the highest interference are arranged as shown in Fig. 3 (grayed nodes). Notice that the nodes in the immediate vicinity of the source do not experience interference since they are directly informed by the source in the first step of the propagation. Finally, notice that there exist four nodes (denoted in bold) that act as data gateways to their respective quadrants. Assume a simple trivial signaling protocol that can switch nodes on/off. (Actual implementation is beyond our scope). Then, the source can direct the dissemination towards specific directions. For example, shutting down the gateways of quadrants 2 to 4 would cause the directed data dissemination towards “North-East”. The potential for directional data routing is discussed further in Section 7.3.

4 SYMMETRY AND PATTERNS IN DENSER GRIDS

The preceding Section studied the patterns formed by nodes with low reception quality in the sparsest connected grid topology. A more robust approach against manufacturing flaws would be to increase the connectivity of the nodes. Thus, the present Section will study the case of denser grids. The connectivity radius of the nodes remains the same, but the size of the square cells decreases. Therefore, each node has an additional number of neighbors, apart from the eight closest ones. Evidently, the Diophantine system methodology is not appropriate for analyzing reception quality patterns in this case.

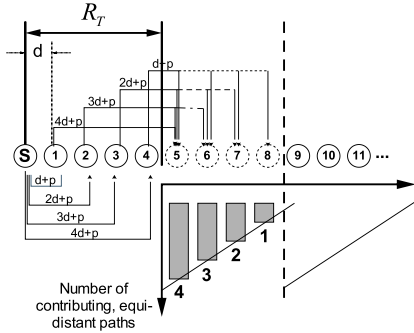


Figure 4: Flood-based propagation of packets via nodes arranged on a line. The propagation delay between two adjacent nodes is d , while the duration of the packet is denoted as p in time units.

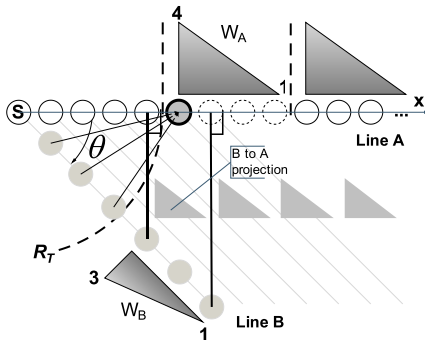


Figure 5: Interactions between two lines of nodes forming an angle θ . The triangular waveforms represent total contributing paths arriving at each node, as in Fig. 4. In general, two separate series on nodes (lines A and B) cause interference to each other. The interference $line\ B \rightarrow line\ A$ can be expressed as the projection of the waveform of B on line A. The phenomenon is recreated indefinitely across line A, due to the presence of other lines of nodes parallel to B.

As a prerequisite to analyzing the complete formed graph, we study the phenomena taking place on a single line of equidistant nodes (Fig. 4). At the initiation of the packet flood, all nodes in the range R_T of the source “s” receive the given packet. Notice that the reception times differ per node, as depicted in Fig. 4. Upon completion of the reception, each of these four nodes re-transmits the packet inside its radius. Notice that all four packets from nodes n_{1-4} arrive to node n_5 at time $5d + 2p$, contributing to the quality of the reception. The same applies to nodes n_{6-8} , noticing that the total number of contributing paths decreases linearly from 3 to 1. The phenomenon is repeated periodically for the remaining nodes on the line, noticing that all nodes receive the given packet successfully.

Remark 2. In flood-based packet propagation via equidistant nodes placed on a line, the reception quality varies periodically. The period and the amplitude of the reception quality are equal to the number of nodes in the connectivity radius.

The introduction of an additional line (B) of nodes at an angle θ is depicted in Fig. 5. The line introduces packet propagation paths leading to line A from the source “s” via line B. These paths have different lengths

than the direct paths via line A. Thus, line B causes interference on line A in the general case. Additionally, we make the following remarks:

Remark 3. Due to the employed grid layout, the distance between nodes on line B differs from that of line A. We denote the number of nodes within radius r on a line at angle θ from the x -axis as $N(r, \theta)$. In the example of Fig. 5 it holds that $N(\widehat{R_T}, \pi/4) = 3$ while $N(\widehat{R_T}, 0) = 4$. In accordance with Remark 2, the reception quality waveform on line B (w_B) has shorter period and amplitude than that of line A.

Remark 4. Consider the sixth node on line A (bold). The node receives a number of $N(\widehat{R_T}, \pi/4)$, generally interfering transmissions from line B, as shown in Fig. 5. The seventh node receives $N(\widehat{R_T}, \pi/4) - 1$ interfering paths, etc. Thus, the interference of line B on line A can be approximated by a projection of the reception quality waveform w_B on line A.

Remark 5. The interference of line B on line A is expected to be periodic, since there exist multiple lines parallel to line B that recreate the phenomenon.

Based on these observations, we can approximate the interference level at a given point of the grid.

Theorem 6. Assume a square grid layout of an indefinite number of nodes. Define a system of polar coordinates originating from the flood-triggering node (source “s”). Let R_T be the connectivity radius of each node. The reception quality, Q , of a node placed at polar coordinates (v, ϕ) is approximated as:

$$Q(v, \phi) = \left| F_{2D} \left\{ \sum_{\forall \theta \in [0, 2\pi) : N(\widehat{R_T}, \theta) \neq 0} I(r, \theta) \right\} \right| \quad (10)$$

where F_{2D} is the two-dimensional Fourier transform, $|\cdot|$ is its amplitude and

$$I(r, \theta) = \begin{cases} N(\widehat{R_T}, \theta) - r, & r \in [0, R_T] \\ 0, & \text{else} \end{cases} \quad (11)$$

Proof: At first, the derivation of $I(r, \theta)$ is explained. In accordance with Remark 2 and Fig. 4, the reception quality on a single line at angle θ from the x -axis is a sawtooth-shaped waveform with amplitude and period equal to $N(\widehat{R_T}, \theta)$. The quantity

$$I(r, \theta) = N(\widehat{R_T}, \theta) - r, \quad r \in [0, R_T] \quad (12)$$

is the expression of the first period of this sawtooth wave. The summation:

$$\ell(r, \theta) = \sum_{\forall \theta \in [0, 2\pi) : N(\widehat{R_T}, \theta) \neq 0} I(r, \theta) \quad (13)$$

is simply the 3D surface $(r, \theta) \rightarrow z$ that comprises all sawtooth waveforms, for every valid angle θ . The notation $\theta \in [0, 2\pi) : N(\widehat{R_T}, \theta) \neq 0$ defines the value set

of angle θ , implying that there exist only discrete angles values for which $N(\widehat{R_T}, \theta) \neq 0^2$. The angles $\theta = 0, \pi/2$ can also be excluded, since Lemma 1 implies that they always correspond to low reception quality.

We proceed to explain the use of the 2D Fourier transform in equation (10) by studying its physical meaning. The continuous F_{2D} of a discrete function $f[x, y]$ is typically expressed in Cartesian coordinates as:

$$F_{2D}(u, m) = \sum_{x=-\infty}^{+\infty} \sum_{y=-\infty}^{+\infty} f[x, y] \cdot e^{-j2\pi(xu+ym)} \quad (14)$$

A grid of points with unary-sized cells over the $x - y$ plane is assumed. The complex exponential can be rewritten as:

$$e^{-j2\pi(xu+ym)} = e^{-j2\pi w(xu/w+y m/w)} = e^{-j2\pi w(\vec{r} \cdot \vec{n})} \quad (15)$$

where $w = \sqrt{u^2 + m^2}$, \vec{n} is the unit vector along the direction (u, m) and \vec{r} is the vector along the direction (x, y) . The inner product $\vec{r} \cdot \vec{n}$ represents the projection of all points (x, y) on the direction of \vec{n} . Using $\ell(r, \theta)$ as $f[x, y]$, all sawtooth-shaped waveforms, representing reception quality at every single angle θ , are projected on the studied direction defined by $\vec{n} = (u, m)$. The contribution level of the projected waveforms is defined by the synchronization of their $e^{-j2\pi w(\vec{r} \cdot \vec{n})}$ sinusoids. Furthermore, the double summation of equation (14) means that the projections are repeated for every point on the direction of \vec{n} , regardless of its distance from the origin. Thus, in accordance with Remarks 3-5, the described two-dimensional Fourier transform approximates the final reception quality at a given point (u, m) , or (v, ϕ) in the equivalent polar coordinates. \square

Remark 7. The reception quality, $Q(v, \phi)$, is quantified as the synchronization level (phase) of message paths that lead to a given node. This is due to equation (13) and the summation of the $e^{-j2\pi w(\vec{r} \cdot \vec{n})}$ factors. However, the analysis does not strictly discriminate between useful and interfering signals, since the exact timing of the packet transmission events is not taken into account. Thus, high $Q(v, \phi)$ values can express either of the following:

- Highly synchronized interference, leading to packet loss, or
- Highly synchronized useful signals.

The dominant condition holds universally, i.e. for the complete topology, excluding the other altogether. Regardless of the case, the goal of the $Q(v, \phi)$ metric is to predict the general form and symmetry of the resulting pattern of trained nodes. This is accomplished in any case. Should it correspond to high interference, the nodes in question are positioned at the local maxima of $Q(v, \phi)$. In the opposite case, they are expected to be at the positions of the local minima.

2. The reader may refer to literature related to the Gauss circle problem, i.e. counting lattice points within a given radius around the axes origin [20]. $N(\widehat{R_T}, \theta)$ is non-zero iff the tangent of θ is rational, $\tan(\theta) = k/l, l \in \mathbb{Z}^*$, and it holds that $\sqrt{k^2 + l^2} < q \cdot R_T$, where $q = \gcd(k, l)$.

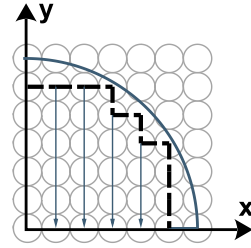


Figure 6: Visualization of the exact definition of $\widehat{N}(r, \theta)$ by iterating over all lattice points (nodes) within the given radius.

A useful property of the patterns of nodes is symmetry. It derives from Theorem 6, noticing that $Q(v, \phi)$ exhibits the same symmetry as $\widehat{N}(r, \theta)$ with regard to the angle θ . Furthermore, it is easily observed from Fig. 3 that $\widehat{N}(r, \theta)$ is symmetric with regard to the lines defined by the angles $\theta = 0, \pi/4, \pi/2$, leading to the following Lemma.

Lemma 8. (*Symmetry property*) The reception quality, Q , of a node placed at coordinates (v, ϕ) is ϕ -symmetric as follows:

$$Q(v, \phi) = Q(v, k \cdot \frac{\pi}{2} \pm \phi), k = 0, 1, 2, \dots \quad (16)$$

This property will be shown to be critical for detecting the position of the packet origin “s” in Section 7.3.

However, the most important property derived from the $Q(v, \phi)$ metric, is that the manifesting patterns extend infinitely across the 2D plane. At first, we make use of the symmetry property of Lemma 8. We notice that $Q(v, \phi)$ is produced from a superposition of sawtooth waveforms, $I(r, \theta)$, each rotated around the z axis. Due to the symmetry property, each sawtooth waveform rotated by an angle θ_o has a symmetric one at angle $\pi + \theta_o$, thus forming an isosceles triangle. The 2D Fourier transform of such a triangle is a sinusoidal surface, whose minima and maxima repeat indefinitely over the plane. The $Q(v, \phi)$ metric is then simply the superposition of several sinusoidal surfaces. Therefore, it will yield optima pseudo-periodically, indefinitely over the plane.

Corollary 9. (*Scalability property*) The pattern formed by the nodes experiencing high interference extends indefinitely over the grid, regardless of their total number.

This property will be shown to ensure the ultra-scalability of the proposed nano-networking scheme.

5 FORMULATIONS OF $\widehat{N}(r, \theta)$

According to Theorem 6, the quantity $\widehat{N}(r, \theta)$ defines the pattern of nodes experiencing high interference. However, deriving a formula for the number of nodes within radius r , on a line θ is not straightforward.

An exact definition can be derived by iterating over all nodes within the given radius, as shown in Fig. 6. For each integer $x = 0 \dots \lfloor r \rfloor$ we calculate the corresponding integer y -value nearest to the circumference

of the circle as $y_m(x) = \lfloor \sqrt{r^2 - x^2} \rfloor$. Finally, the points $\{x, 0 \dots y_m(x)\}$ are iterated as denoted by the vertical arrows in Fig. 6, logging the corresponding angles $\tan^{-1}(y/x)$. We produce:

$$\widehat{N}(r, \theta) = \sum_{x=0}^{\lfloor r \rfloor} \sum_{y=0}^{\lfloor \sqrt{r^2 - x^2} \rfloor} \delta\left(\theta - \tan^{-1}\left(\frac{y}{x}\right)\right) \quad (17)$$

where $\delta(\cdot)$ is Kronecker's delta function. A similar formulation is used for solving exactly the "circle problem" proposed by Gauss [20, p. 39].

Iterating over all nodes may not be practical for high values of r . An alternative formulation is proposed for these cases:

Theorem 10. *Assuming a square grid layout, the number of nodes within a large radius r from the axis origin on a line θ is given by:*

$$\widehat{N}(r, \theta) \approx \frac{r}{\arg \min_{(R \in (0, r])} \left\{ \sqrt{2R \cdot (s_1 \cdot \cos\theta + s_2 \cdot \sin\theta) + R^2} - R \right\}} \quad (18)$$

where $s_1 = \text{SawTooth}[R \cdot \cos\theta]$ and $s_2 = \text{SawTooth}[R \cdot \sin\theta]$ are periodic functions such as $\text{SawTooth}[x] = -x, x \in [0, 1]$.

Proof: Equation (18) calculates $\widehat{N}(r, \theta)$ by dividing the given radius r by the distance of the node on line θ that is closest to the axes origin.

Firstly, we express the dashed curve of Fig. 6 in polar coordinates. For an arbitrary radius R :

$$\mathcal{D}(\theta) = \sqrt{\lfloor R \cos\theta \rfloor^2 + \lfloor R \sin\theta \rfloor^2} \quad (19)$$

As R increases, $\mathcal{D}(\theta)$ becomes approximately equal to R for any angle θ . Let $\Delta(\theta) = \frac{\mathcal{D}(\theta)^2}{R^2} - 1$. It holds that:

$$\lim_{R \rightarrow \infty} \Delta(\theta) \rightarrow 0 \quad (20)$$

Additionally, by substituting $\lfloor R \cos\theta \rfloor$ and $\lfloor R \sin\theta \rfloor$ with the equivalent expressions $R \cos\theta + s_1$ and $R \sin\theta + s_2$, $\Delta(\theta)$ can be rewritten as:

$$\Delta(\theta) = \frac{s_1^2 + s_2^2 + 2R(\cos\theta \cdot s_1 + \sin\theta \cdot s_2)}{R^2} \quad (21)$$

Notice that

$$\lim_{R \rightarrow \infty} \Delta(\theta) \cdot R \rightarrow 2(\cos\theta \cdot s_1 + \sin\theta \cdot s_2), \neq 0, \infty \quad (22)$$

which is periodic. Equations (20) and (22) are the prerequisites for the Periodicity Extraction Technique of [21]. According to it, $\lim_{R \rightarrow \infty} \Delta(\theta) \cdot R \approx \Delta(\theta) \cdot R$, since $\Delta(\theta) \cdot R$ is periodic. Thus, from equation (22), $\Delta(\theta)$ is simplified as:

$$\Delta(\theta) \approx \frac{2(\cos\theta \cdot s_1 + \sin\theta \cdot s_2)}{R} \quad (23)$$

The curve $\mathcal{D}(\theta)$ is then written as:

$$\mathcal{D}(\theta) \approx \sqrt{\Delta(\theta) \cdot R^2 + R^2} = R\sqrt{\Delta(\theta) + 1} \quad (24)$$

The quantity $\mathcal{D}(\theta) - R$ is the deviation of the last lattice point on line θ from the circumference R . Consider all values of $R \in (0, r]$ and a given angle θ . The value $R = R_o$ that minimizes the deviation $\mathcal{D}(\theta) - R$ is the distance of the first lattice point from the origin, on line θ . Finally, $\widehat{N}(r, \theta)$ is calculated as the ratio r/R_o , QED. \square

Theorem 10 serves as an additional proof of Lemma 8 regarding the symmetry of the patterns of nodes. Notice that the quantity $\cos\theta \cdot s_1 + \sin\theta \cdot s_2$ in the denominator of equation (18) remains unchanged when substituting θ with $k \cdot \frac{\pi}{2} \pm \theta$.

Additionally, a metric representing the *angular density* of lattice points can be derived from equation (18) as:

$$\rho(\theta) = \frac{\widehat{N}(r, \theta)}{r} \approx$$

$$\arg \min_{(R \in (0, \infty])} \left\{ \sqrt{2R \cdot (s_1 \cdot \cos\theta + s_2 \cdot \sin\theta) + R^2} - R \right\}^{-1} \quad (25)$$

To the best of the authors' knowledge, the metric $\rho(\theta)$ is quantified for the first time in point lattice algebra. The s_1, s_2 sawtooth functions can be substituted by their Fourier series, which are conveniently expressed as sums of $\sin(\cdot)$ factors only. Taking into account only the first N factors, the argument of the *argmin* operator can be seen as a continuous function of R and can be handled by any numerical solver.

6 EXPLOITING NODE PATTERNS FOR ULTRA-SCALABLE NANO-NETWORKING

The analysis of Sections 3 and 4 showed that the nodes that experience low reception quality form symmetric patterns around the packet origin. This phenomenon can be exploited for applying an ultra-scalable node specialization scheme. Nodes that experience good reception quality can come to serve as packet retransmitters ("*network infrastructure*"), while the remaining nodes can revert to read-only mode ("*users*"). The "*infrastructure*" is also expected to consist of lines of nodes originating from the packet source (Theorem 6), extending indefinitely (Corollary 9). Thus, wide coverage and indefinite scalability are expected, as well as significant gains in energy-efficiency, since the "*users*" do not retransmit messages.

The classification of nodes is described as a maturity process, running locally on each node. The process is an adaptation of the Dendritic metaheuristic proposed in [22] and is described by the state transition diagram of Fig. 7. All nodes are initially immature. In this state a node retransmits all incoming messages, collecting experience. The training occurs with each packet reception, either successful or not. Each node is initialized to null training status (*current_experience* scalar variable). We assume that the ratio of the useful signal power to the combined power of interference and noise (SINR ratio) defines the reception of a given packet. While receiving each incoming packet, a node measures:

- The mean observed Interference level, I .
- The mean observed Signal level, S .

Other definitions can also be freely used. As an example of a stricter definition, S can represent the minimal observed signal level, while I can be the maximal interference level during the reception of a packet. In addition, the illustration assumes a constant noise level throughout the nano-network. Should the noise vary, the I metric should be simple updated to $I + N$ where N is the noise level.

The aggregate signal power, $S + I$, represents the signal processing experience of the node and is used for advancing the *current_experience* index. In the meantime, a simple index of signal quality (*current_bias*) is updated by an amount of $S - 2 \cdot I$. Notice that the form of the update rules is very simple, as defined universally in [22]. Should the *current_experience* exceed a given threshold T and *current_bias* be positive, the node becomes a part of the network infrastructure, retransmitting incoming packets. If *current_bias* is negative, the node becomes a single “user”. The threshold T is an input parameter, but is not expected to require special tuning. It defines the training speed of the nanonodes. For immobile nodes, any appropriately large value can capture the reception quality statistics of a node. For dynamic topologies, T could be picked at random, between a very small and a very large value. For example, the maturity threshold of any node can be set to a random value corresponding to the processing of 10 to 1000 packets. The actual T value can be derived from static network attributes, such as containing space dimensions, average node density, packet duration and Tx power level. In this way, the long-term and short-term dynamics of the topology can be captured by the training process.

As the maturity procedure proceeds, several nodes may quickly turn into “users”, limiting the interference to their still “immature” neighbors. This effect may alter the expected pattern of nodes, since nodes that were supposed to become “users” may eventually turn into “infrastructure”. The phenomenon affects sparse networks (e.g. 10 neighbors per node), since the input from each of the neighbors is significant. In denser networks (with e.g. more than 50 neighbors) this effect is negligible and disappears altogether for higher density values. If this effect on sparse networks is unwanted, it can be resolved in a very simple manner: If a node turns into a “user”, it can still act as a blind retransmitter for a constant time interval (i.e. a timeout). Thus, all neighbors have enough time and input to reach the expected maturity state. This approach is followed successfully in the ensuing simulations of sparse networks (8 neighbors).

Notice that the training process is simple, including only comparisons, additions and subtractions in the strict mathematical sense. This is inline with the low complexity restrictions imposed by the nano-scale. Finally, it is worth mentioning that the maturity process can be easily made continuous and dynamic [22]. In

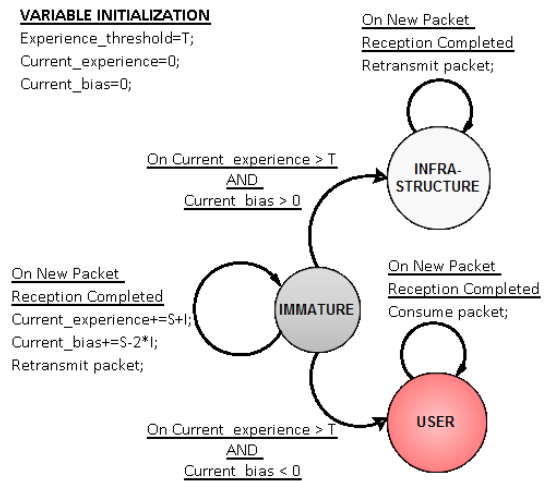


Figure 7: The maturity process of a given node. The node matures to assume the role of “infrastructure” or “user” based on its SINR readings during the reception of packets.

order to achieve this, the classification result may be invalidated after a time-interval. This approach would enable state transitions from the “infrastructure” and “user” states back to “immature” after a timeout, repeating the maturity process anew. While initial results are provided in the simulations Section, extensive research on this subject is the focus of future work.

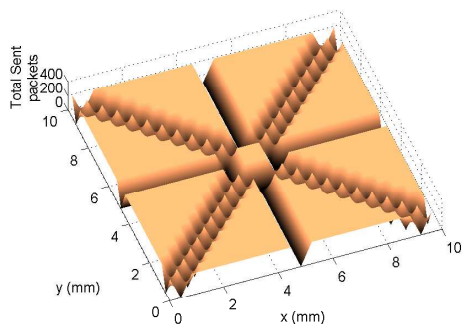
7 SIMULATIONS

In this Section, the theoretical expectations regarding the patterns of nodes and their attributes are compared to simulation-derived results. Furthermore, the benefits of the proposed scheme are presented and compared to optimal flood and MAC-based packet propagation. The comparison considers the metrics of: i) achieved coverage (mean percentage of successfully informed nodes, calculated over all distinct packets emitted by the source), ii) mean service time per node (i.e. the mean time required to relay a packet to each of the covered nodes), iii) Packet sending, reception and collision rates over all nodes for the duration of the simulation. Notice that the packet sending rate also expresses the energy efficiency of the network. In addition, further exploitations of the node patterns are demonstrated. Applications on data routing and packet origin discovery are demonstrated. Both lattice-arranged and random topologies are studied.

The simulations are implemented on the AnyLogic platform [23]. The persistent simulation attributes are given in Table 1. The propagation parameters are typical for studies on nano-networks [6]. A two dimensional layout of nodes is assumed, while their number varies per experiment. A source, placed at a position specified per experiment, periodically generates and broadcasts packets. Each node that receives a packet for the first time retransmits it in its radius. In the meantime, the *Current_experience* is updated as described. At time

Table 1: Persistent Simulation Parameters

Parameter	Value
Area of Study	$10 \times 10\text{mm}$
Frequency	100GHz
Tx Power	10nW
Noise Figure	0dB
Node Sensitivity ($SINR_{\text{thresh}}$)	-10dB
Attenuation Model	Free Space
Packet Duration	10nsec
Packet Inter-arrival (source)	20nsec
Simulation Duration	$60\mu\text{sec}$
Maturity Decision at:	$30\mu\text{sec}$
Experience Threshold	300nW

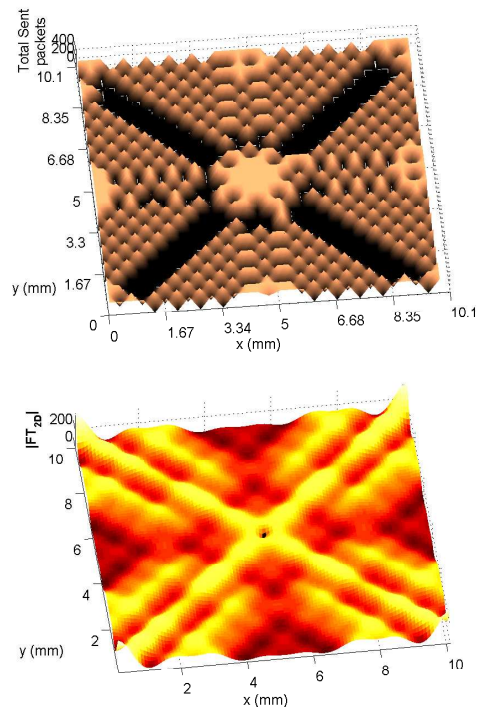
**Figure 8:** Pattern of infrastructure nodes manifesting at a grid layout of 625 nodes. The metric of node activity is the total number of packets sent during the simulation.

$t = 30\mu\text{sec}$, the nodes begin to operate by their maturity status. This time limit is employed for clearly measuring the impact of the proposed scheme. All presented measurements refer to the time interval from $t = 30\mu\text{sec}$ to the end of the simulation at $t = 60\mu\text{sec}$.

The following experiments consider the cases of $n = 625$, 900 and 4000 nodes positioned on the described area of study. The first case corresponds to the sparsest connected grid, studied in Section 3. The latter two cases correspond to the denser grids of Section 4. The definition of the I and S metrics of Fig. 7 varies per case. For $n = 625$, each node is connected to just 8 neighbors (as in Fig. 3). Therefore, since dependable mean values are hard to derive, I is better expressed as the maximum interference level during a reception, while S is the minimum useful signal level. For $n = 4000$ the number of neighbors is ~ 80 and mean values can be used. The case of $n = 900$ is transitional (30 neighbors per node) and we set I to be the mean interference and S the minimum useful signal level. Notice that these choices are made for practical reasons regarding the simulations. One could use mean values in any case, but prolong the duration of the node training interval in order to derive dependable values.

7.1 Symmetry: Expected and observed node patterns

Firstly, we examine the case of $n = 625$ nodes, uniformly arranged (25×25) over the area of study. The source

**Figure 9:** Expected (lower graph) and derived (upper graph) patterns of infrastructure nodes. The network comprises 900 nodes in grid layout. The general form and symmetry of the expectation approximate the pattern derived through simulations. Notice that the duality of the graphs is in accordance with Remark 7.

(periodic packet beacon) is placed at the center of the plane. Placing the source at other positions introduces a simple offset to the presented Figures, with no other consequence. We log the total number of packets sent by each node during the interval of measurements. The results are given as the surface plot of Fig. 8. Black spots correspond to simple “users” (zero sent packets), while orange ones to “infrastructure”. The manifesting pattern is in exact accordance with the theoretical expectation of Fig. 3. A critical point to stress out is that all presented patterns were observed to extend indefinitely, regardless of the number of nodes, validating the scalability property of the proposed scheme.

In Fig. 9 the number of nodes is raised to $n = 900$. Since each node is connected to approximately 30 neighbors, we employ Theorem 10 to predict the new pattern of nodes. The prediction is given at the lower part of the Figure, while the experimental results are given at the upper part. The local minima and maxima of the expected pattern correspond to the simulation-derived pattern. Notice that the mean amplitude of the 2D Fourier transform approximates the mean number of sent packets per node (~ 200). However, this phenomenon should be considered coincidental and is beyond the scope of the present study. The recommended use of the expected patterns is to predict the locations of nodes experiencing low reception quality based on the local optima of the plots. As an additional note, more than $\sim 50\%$ of the nodes turn into passive users, not

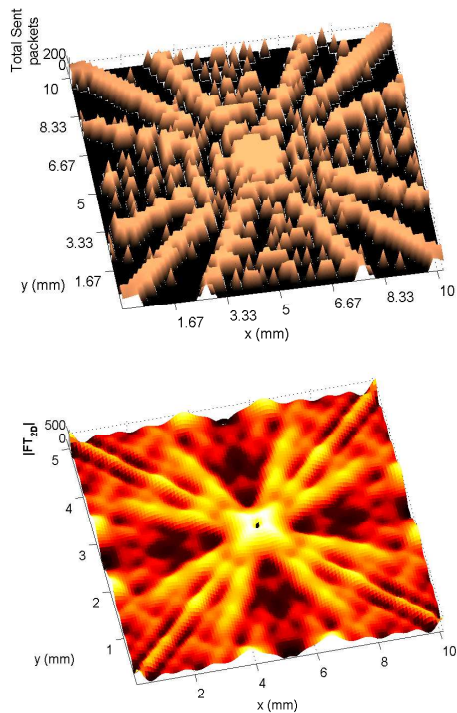


Figure 10: Expected (lower graph) and derived (upper graph) patterns in the case of 4000 nodes. A star-like symmetry manifests regarding the positions of the “infrastructure” nodes. The graphs match, while more than 60% of the nodes turn into passive users.

retransmitting any messages during the measurement interval. This phenomenon is also highly valuable in terms of energy-efficient nano-networking. Notice that nano-machines are expected to face multiple restrictions in terms of energy expenditure.

The accordance between the expected pattern and the experimental results is also evident in the case of $n = 4000$ nodes (Fig. 10). The network is much denser in this case, with each node having approximately 80 connected neighbors. Theorem 10 projects the radial distribution of infrastructure nodes with good accuracy. Furthermore, the experimental results indicate that more than 60% of the nodes turn into “users”, increasing the energy efficiency of the network further. As expected, the number of “user” nodes increases as the network becomes denser. A dense network has a high number of redundant connections. Turning several nodes to simple users limits this redundancy, without any effect on the achieved coverage.

7.2 Efficiency: Comparison to Optimal Probabilistic and MAC-based Flood

Operating at nano-scale restricts the computational complexity of a candidate communication scheme. Two prominent, lightweight solutions, originating from the field of wireless sensor networks, are the optimal probabilistic and the CSMA/CA-based packet flood. This Section compares these alternatives to the proposed scheme that functions as “dynamic infrastructure” deployment.

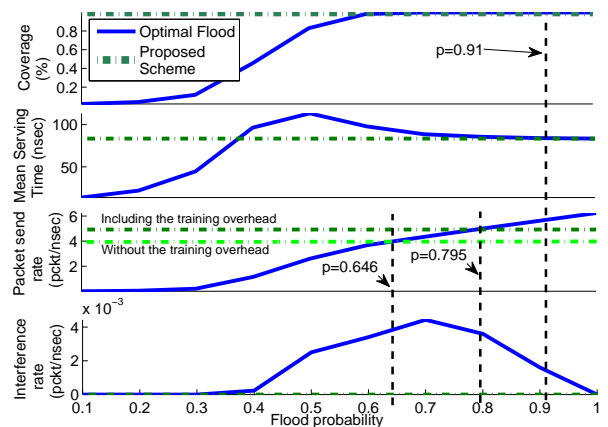


Figure 11: Comparison of efficiency between the proposed scheme and optimal probabilistic flooding. The dynamic infrastructure offers optimal coverage and service times with lower energy expenditure, even when including the training overhead. In addition, it does not require any optimization.

Figure 11 presents the comparative performance between the proposed scheme and the probabilistic flood. The comparison considered $n = 625, 900$ and 4000 nodes in uniform and random layouts over the study area. Similar conclusions were derived in each case. Due to space restrictions, only the case of $n = 625$ uniformly arranged nodes is given in Fig. 11.

According to the probabilistic flood paradigm, each node retransmits a new incoming packet with probability p . Optimality refers to the fine tuning of the p parameter. It has been observed that increasing p beyond a certain value for a given network is fruitless [24]. The superfluous retransmissions increase the collision rate and the energy expenditure with little to no gain in coverage or service time. Choosing the optimal value for p requires each node to have at least partial knowledge of the state of the network [16]. While this requirement is rather ambitious for nano-networks, we exhaustively compare every possible p value to the proposed scheme.

The comparisons consider the setup of Section 7.1 for both competing schemes (Table 1). The maturity status is simply neglected while simulating the probabilistic flooding. The interval of measurements remains the same. We measure the achieved coverage (percentage of nodes that get a given packet emitted by the source), the coverage time, the packet sending and interference rate. As shown in Fig. 11, probabilistic flood achieves optimal performance for $p = 0.91$. However, the formation of dynamic infrastructure already achieves this level of coverage/service time, but with less sent packets, while yielding null interference events. Energy-efficiency is thusly promoted. In essence, the trained network combines the performance of $p = 0.91$ with the energy efficiency of $p = 0.795$ (or $p = 0.646$ when excluding the training overhead of $0-30\mu sec$). The results remain similar when varying the number of nodes and randomizing their layout.

From another aspect, the dynamic infrastructure can

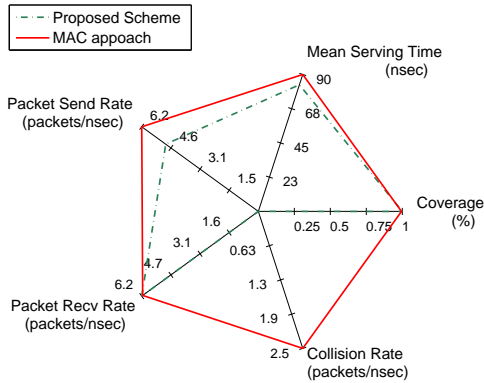


Figure 12: Comparison between a trained network (proposed) and a MAC-based approach. Both schemes achieve 100% coverage. The trained network offers better coverage times, smaller energy expenditure rate and zero interferences.

be seen as an automatically fine-tuned probabilistic flood. Turning several nodes to “users” is tantamount to setting their retransmission probability to 0. Meanwhile, the “infrastructure” nodes use a probability $p = 1$. Qualitatively, this outcome corresponds to a global average p that is less than 1, approaching optimality automatically. However, optimal flooding implies no symmetry or manifestation of patterns of nodes, which will be shown to have useful applications in Section 7.3.

Comparison with a CSMA/CA approach (Carrier-Sense Multiple Access with Collision Avoidance) takes place in Fig. 12-14. CSMA/CA is a simple MAC protocol which is extensively used in the IEEE 802.11 standard. According to it, a node senses the channel availability before transmitting a packet. If the channel is not free, the packet is buffered and the transmission is postponed for a random back-off interval. If the channel is free, the sender and the receiver exchange RTS/CTS signals (ready-to-send, clear-to-send) and the transmission begins. Notice that this mechanism implies added node complexity. Apart from the carrier sense and packet buffering capabilities, the RTS/CTS mechanism needs to be implemented at nanoscale, along with a node addressing scheme. Since such complexity is prohibitive for the studied networks, we consider a lightweight variation of CSMA/CA which does not include the RTS/CTS exchange. The carrier sensing and buffering capabilities are retained. We assume that each node is equipped with a queue capable of accommodating 10 different packets, while the back-off interval is picked uniformly at random in $(0, 10]nsec$. In other words, its maximum value is equal to the size of the packets. The setup and measured metrics are as already described. Figures 12-14 refer to uniform layouts, but similar results are derived for random arrangements as well.

Dynamic infrastructure offers better performance with less expended energy in every case. At $n = 625$ nodes (Fig. 12), the proposed scheme provides perfect

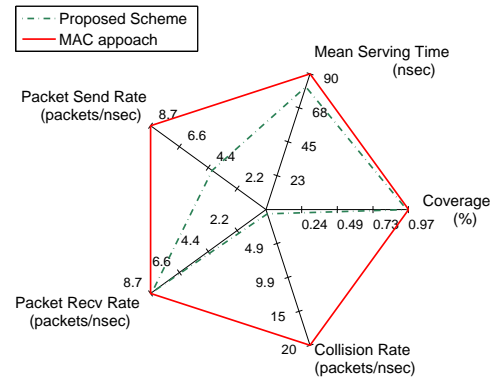


Figure 13: In a denser network (900 nodes), the performance gap between the trained network and the MAC approach widens. The energy expenditure is reduced to 50% of the MAC approach, while interference events are still near-zero.

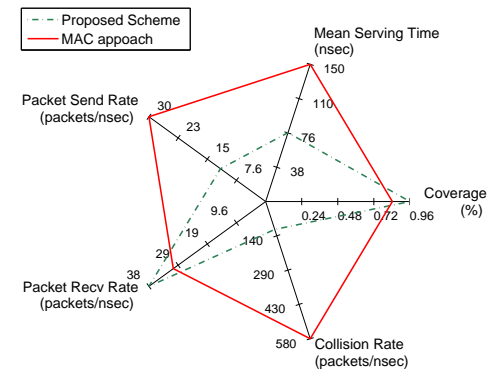


Figure 14: In even denser networks (4000 nodes), the trained network offers clearly better performance (coverage, service time) and smaller energy expenditure rate.

coverage-just like the MAC-based approach-but better service times. However, this combination is achieved with zero packet collisions and by sending just the 75% of the total number of packets with regard to the MAC approach. Increasing the number of nodes widens the performance gap in favor of the dynamic infrastructure. At $n = 900$ nodes (Fig. 13), the proposed scheme offers better performance and expends half of the energy required by the MAC scheme. The collision rate is still near-zero. For $n = 4000$ (Fig. 14) the performance gap is much wider. The coverage of the MAC approach has dropped to $\sim 80\%$ while the proposed scheme achieves 100%. Furthermore, dynamic infrastructure offers half the service time, $\sim 80\%$ less collisions and requires 55% less energy.

Evidently, attributing buffering capabilities to the nodes makes the wireless channel occupied for extended periods of time. Furthermore, it does not promise substantial benefits, since the surrounding nodes may have already received the buffered messages. A MAC scheme

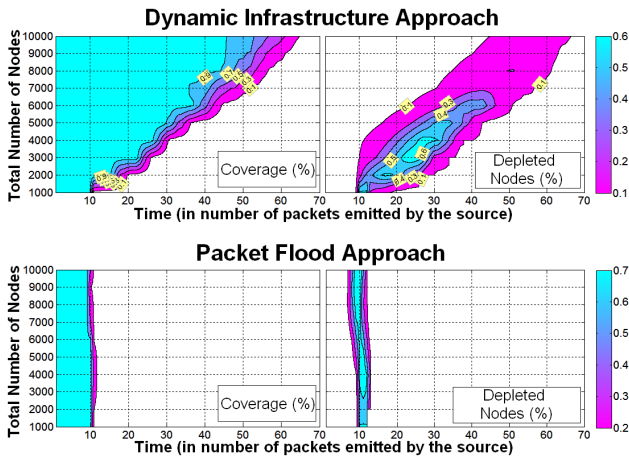


Figure 15: Network lifetime comparisons between the proposed scheme and packet flooding, examining various cases of network density. In packet flooding, the network ($\approx 70\%$ of the nodes) dies abruptly early on. The dynamic infrastructure extends its lifetime considerably in any case. In addition, it maintains a high number of powered nodes (up to 90%), even when the source loses connectivity to the network when its immediate neighbors die out.

might behave better in a scenario where the nodes could exchange signals on their status and needs. Since a nano-network cannot offer such commodities, MAC-based solutions may not constitute viable choices when compared to the proposed scheme.

It is also worth noting the gains in network lifetime, achieved by the dynamic infrastructure. In Fig. 15 we assume a random (uniform) topology for a set of node density cases (y-axis ticks). We assume further that a node dies-out when it transmits 10 packets, while the maturity process is dynamic, as discussed in Section 6. The source is placed in the middle of the topology and all other attributes are the same as in the previous simulations. For every distinct packet emitted by the source (x-axis), we log the coverage (percentage of powered nodes that received the message successfully) and the percentage of energy-depleted nodes. The Figure presents the mean results derived from 50 simulation repetitions with random topologies. The packet flood approach achieves high coverage, but limited lifetime. Most of the nodes ($\sim 70\%$) die out in minimal time. The dynamic infrastructure has two benefits. At first, it extends the lifetime of the network considerably in all cases, with no compromise in terms of coverage. Secondly, when the network gets eventually segmented (e.g. when the immediate neighbors of the source die out), most of the nodes are still powered-up (up to $\sim 90\%$). This means that the network maintains a high degree of serviceability even under stress, a trait that is expected to be particularly valuable in the dynamic topologies (mobile nodes) that are presently under study.

7.3 Applications: Data routing and Source location discovery

The symmetry of dynamic infrastructure, manifesting during the operation of the system makes for further

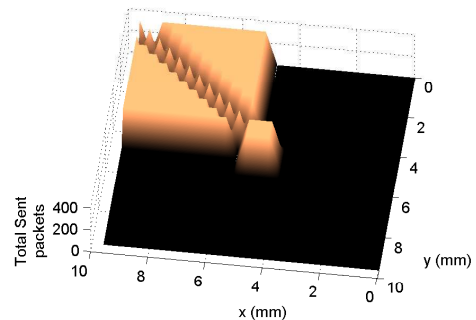


Figure 16: By shutting down just three nodes, the layout of Fig. 8 transforms to a directed propagation scheme. Packets are transmitted only towards the “North-Western” quadrant. This can be perceived as a kind of virtual beam forming. Furthermore, assuming a proper signaling protocol, the source can choose the propagation path, essentially routing information as required.

useful applications. Certain cases of arranged networks enable the routing of data in manner resembling beam-forming techniques. Furthermore, the dynamic infrastructure can be used for approximating the location of the packet origin, in both arranged and random topologies, by performing simple power measurements at the perimeter of the network.

Concerning the data routing capabilities, we consider the case of $n = 625$ uniformly arranged nodes. As discussed, the pattern of nodes corresponds to Fig. 3. In this Figure, we observe that the four nodes denoted in bold supply their respective quadrants with packets. In other words, they serve as gateways, connecting these sectors to the source. Assume that a proper, higher level signaling protocol exists, through which the source can switch any of these four nodes on or off. The source can then effectively choose the propagation path, routing information as required. By shutting down just three nodes, the layout of Fig. 8 transforms to the directed propagation scheme of Fig. 16. Packets are transmitted only towards the “North-Western” quadrant. This data routing can be perceived as a very effective kind of beam forming, since the packet propagation is turned to a specific direction. The true merit of this capability is that it cannot be accomplished by probabilistic flooding schemes. The latter would not have a way of containing the packet propagation in a given sector, despite the directivity of the source’s antenna. This ability is possible due to the form of the infrastructure pattern, as shown in Fig. 3. The applicability to arranged networks could exemplary have potential uses to future, printed nanonetworks.

The discovery of the location of the packet source is another interesting property deriving from the patterns of the dynamic infrastructure. This capability is especially interesting, since nanonetworks are not expected to support close examination of their internals. We therefore assume that the nanonetwork is a black box, being accessible only at its perimeter. As demonstrated in Fig. 8, 9 and 10 the packets are propagated along radial

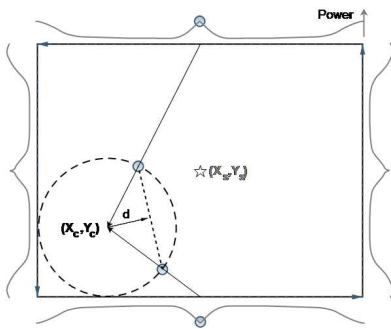
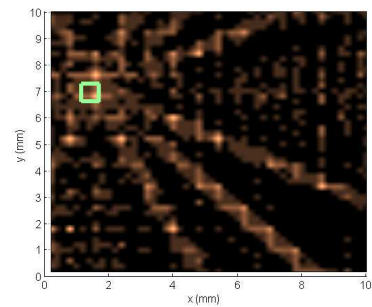


Figure 17: Penalization of candidate source locations based on the lack of symmetry regarding the power peaks on the perimeter of the network.

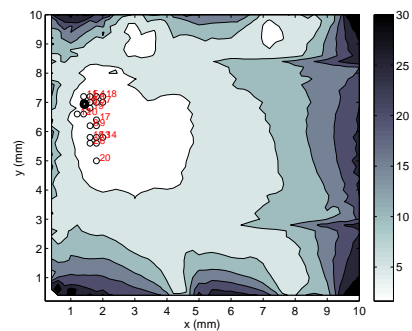
lines originating from the origin. Should we measure the emanating power on the perimeter of the network, it is expected that certain local maxima will be encountered. An illustration is given in Fig. 17. These local maxima should be symmetric, in accordance with Lemma 8. For simplicity, we examine only their π -symmetry. In order to detect the most prominent source location we define an algorithm that penalizes unfit candidate locations. At first, we define the biggest circle registered in the network area and project the detected local optima on its circumference, as shown in Fig. 17. If the candidate point (X_c, Y_c) coincided with real source coordinates at (X_s, Y_s) , the projections would be π -symmetric and the length of interval d would be zero. Therefore, the aggregate d intervals over all symmetric pairs of maxima can serve as a penalty (or unfitness) for choosing the candidate point as the prominent location of the source. The pairing of projected optima is accomplished by matching a given local maximum to the one closest to its π -symmetric point on the circle. Finally, the minor optima (e.g. the power peaks below 30% of the global maximum) can be filtered out of the process.

An example of the penalization process is given in Fig. 18. We study the case of a dense network with 4000 uniformly arranged nodes (Fig. 18a). The source is placed at an arbitrary point (square marker). It is assumed that the network is a black box, the location of the source is unknown and we can only perform power measurements on the perimeter of the square area. We traverse the perimeter of the area via the route $(0,0) \rightarrow (10,0) \rightarrow (10,10) \rightarrow (0,10) \rightarrow (0,0)$ and log the power levels on it. Peaks (local maxima) are detected and the minor ones are filtered out. By penalizing all points in the plane, we produce the contour plot of Fig. 18b. The minima of the plot represent the most probable source locations. The circles exemplary denote the twenty lowest values (less penalized points). The location of the source is detected with good precision, while the contour plot exhibits strong convexity.

The convexity of the penalizing scheme is also supported by the results of Monte Carlo tests. Assuming $n = 4000$ nodes and the standard $10 \times 10 \text{ mm}$ study area, we perform 20 runs, each time placing the source at a



(a) An example of source location discovery. We assume a dense network with 4000 nodes. The source is placed at an arbitrary point (square marker). The inner pattern is unknown, but we can perform power measurements on the perimeter of the network. By applying the penalization scheme for each (x,y) point of the network area we form the contour plot of Fig. 18b.



(b) The minima of the formed contour plot (see Fig. 18a) represent the most probable source locations. The circles exemplary denote the twenty lowest values (less penalized points). The location of the source is detected with good precision, while the contour plot exhibits strong convexity.

Figure 18: Employing the infrastructure symmetry for source location discovery.

random point within the study area. The first 10 runs assume the arranged node layout, while the latter 10 operate on random layouts per run. We execute the described penalizing scheme, defining the most prominent source location as the mean over the 20 less penalized points. For each run, we logged the prediction error as the Euclidean distance (in mm) between the expected and the real source location. The mean error in the arranged layout was equal to 1.5442 mm and the standard deviation 0.8159 mm . For random layouts, the mean error was 2.16 mm and the standard deviation 0.6107 .

The precision of the presented penalizing scheme is satisfactory, given its simplicity and its ability to operate in random topologies as well. Furthermore, notice that the scheme took into account only the π -symmetry of the local maxima, while Lemma 1 predicts additional axes of symmetry which could enhance its precision further. Advancing the precision of source detection is in the scope of future work. Nonetheless, the presented results constitute the proposed dynamic infrastructure a promising solution for networking nano-nodes, combining robust, energy efficient communication with interesting applications, all accomplished through a very

lightweight, distributed process.

8 CONCLUSION AND FUTURE WORK

Nano-networking requires low complexity, but ultra-scalability and high efficiency. The present study contributed a multi-modal nano-node networking scheme which upholds these conditions. A single, low complexity nano-node architecture serves multiple roles, including optimal data dissemination, indefinite scalability, promotion of energy-efficiency, directional data routing and protocol-less detection of a data source location. Its operational principle was to classify each node as either infrastructure or single user, depending on its reception quality. Through analysis and simulations it was demonstrated that the infrastructure nodes form regular patterns in grid network layouts. The related analysis also contributed new formulas to point lattice algebra. Exploiting the form of the node patterns, the proposed scheme combined unique applications with superior networking and energy efficiency with regard to alternatives. Due to its extremely low computational requirements, the proposed scheme is expected to constitute a viable networking choice for future nano-network implementations.

REFERENCES

- [1] I. F. Akyildiz and J. M. Jornet, "Electromagnetic wireless nanosensor networks," *Nano Communication Networks*, vol. 1, no. 1, pp. 3–19, 2010.
- [2] F. Albano, Y. Lin, D. Blaauw, D. Sylvester, K. Wise, and A. Sastry, "A fully integrated microbattery for an implantable microelectromechanical system," *Journal of Power Sources*, vol. 185, no. 2, pp. 1524–1532, 2008.
- [3] J. Kong, "Nanotube Molecular Wires as Chemical Sensors," *Science*, vol. 287, no. 5453, pp. 622–625, 2000.
- [4] A. Akkaya and T. Tugcu, "Analog Molecular Communication in Nanonetworks," in *Bio-Inspired Models of Networks, Information, and Computing Systems*, ser. Lecture Notes of the Institute for Computer Sciences, Social Informatics and Telecommunications Engineering. Berlin and Heidelberg: Springer Berlin Heidelberg, 2012, vol. 103, pp. 171–182.
- [5] J. Capdevila Pujol, "Bridging PHY and MAC Layers in Wireless Electromagnetic Nanonetworks," Ph.D. dissertation, Escola Tècnica Superior de Telecomunicacions de Barcelona (ETSETB), Barcelona and Spain, December 13, 2010.
- [6] J. M. Jornet, J. Capdevila Pujol, and J. Solé Pareta, "PHLAME: A Physical Layer Aware MAC protocol for Electromagnetic nanonetworks in the Terahertz Band," *Nano Communication Networks*, vol. 3, no. 1, pp. 74–81, 2012.
- [7] V. Srikanth, S. Chaluvadi, Vani, and Venkatesh, "Energy Efficient, Scalable and Reliable MAC Protocol for Electromagnetic Communication among Nano Devices," *International Journal of Distributed and Parallel Systems*, vol. 3, no. 1, 2012.
- [8] C. Mavroidis and A. Ferreira, "Nanorobotics: Past, Present, and Future," in *Nanorobotics*. New York and NY: Springer New York, 2013, pp. 3–27.
- [9] F. Dressler and F. Kargl, "Towards security in nano-communication: Challenges and opportunities," *Nano Communication Networks*, vol. 3, no. 3, pp. 151–160, 2012.
- [10] J. M. Jornet and I. F. Akyildiz, "Channel Modeling and Capacity Analysis for Electromagnetic Wireless Nanonetworks in the Terahertz Band," *IEEE Transactions on Wireless Communications*, vol. 10, no. 10, pp. 3211–3221, 2011.
- [11] P. Wang, J. M. Jornet, M. Abbas Malik, E. Fadel, and I. F. Akyildiz, "Energy and spectrum-aware MAC protocol for perpetual wireless nanosensor networks in the Terahertz Band," *Ad Hoc Networks*, 2013.
- [12] J.-P. Hubaux, J. J. Garcia-Luna-Aceves, D. B. Johnson, B. Williams, and T. Camp, "Comparison of broadcasting techniques for mobile ad hoc networks," in *Proceedings of the 3rd ACM international symposium on Mobile ad hoc networking & computing - MobiHoc '02, Lausanne, Switzerland, June*. ACM Press, 2002, p. 194.
- [13] H. Kodesh, V. Bahl, T. Imielinski, M. Steenstrup, Q. Hu, D. L. Lee, and W.-C. Lee, "Performance evaluation of a wireless hierarchical data dissemination system," in *Proceedings of the 5th annual ACM/IEEE international conference on Mobile computing and networking - MobiCom '99*. ACM Press, 1999, pp. 163–173.
- [14] S. Crisóstomo, U. Schilcher, C. Bettstetter, and J. Barros, "Probabilistic flooding in stochastic networks: Analysis of global information outreach," *Comp. Netw.*, vol. 56, no. 1, pp. 142–156, 2012.
- [15] Q. Zhang and D. P. Agrawal, "Dynamic probabilistic broadcasting in MANETs," *Journal of Parallel and Distributed Computing*, vol. 65, no. 2, pp. 220–233, 2005.
- [16] H. Shah-Mansouri, M. R. Pakravan, and B. H. Khalaj, "Analytical Modeling and Performance Analysis of Flooding in CSMA-Based Wireless Networks," *IEEE Transactions on Vehicular Technology*, vol. 60, no. 2, pp. 664–679, 2011.
- [17] Chien-Chung Shen, Zhuochuan Huang, and Chaiporn Jaikaeo, "Directional broadcast for mobile ad hoc networks with percolation theory," *IEEE Transactions on Mobile Computing*, vol. 5, no. 4, pp. 317–332, 2006.
- [18] A. Xeros, M. Andreou, A. Pitsillides, and M. Lestas, "Adaptive Probabilistic Flooding for Information Hovering in VANETs," in *Proceedings of the 2010 IEEE Vehicular Networking Conference (VNC 2010), Jersey City, New Jersey, USA, December, 2010*, pp. 121–127.
- [19] K. Kantelis, S. Amanatidis, C. Liaskos, P. Nicopolitidis, N. Konofaos, and G. Papadimitriou, "On the Use of FDTD and Ray-Tracing Schemes in the Nanonetwork Environment," *Aristotle University Digital Library, Technical Report*, 2014. [Online]. Available: <http://caclab.csd.auth.gr/Library/TR/TR4-2014.pdf>
- [20] D. Hilbert and S. Cohn-Vossen, *Geometry and the imagination*. Providence and RI: AMS Chelsea, 1999.
- [21] C. K. Liaskos and G. I. Papadimitriou, "Generalizing the Square Root Rule for Optimal Periodic Scheduling in Push-Based Wireless Environments," *IEEE Transactions on Computers*, vol. 62, no. 5, pp. 1044–1050, 2013.
- [22] J. Greensmith, U. Aickelin, and G. Tedesco, "Information fusion for anomaly detection with the dendritic cell algorithm," *Information Fusion*, vol. 11, no. 1, pp. 21–34, 2010.
- [23] XJ Technologies, "The AnyLogic Simulator," 2013. [Online]. Available: <http://www.xjtek.com/anylogic/>
- [24] Z. Haas, J. Halpern, and Li Li, "Gossip-based ad hoc routing," *IEEE/ACM Trans. on Networking*, vol. 14, no. 3, pp. 479–491, 2006.



Christos Liaskos received the Diploma in Electrical and Computer Engineering from the Aristotle University of Thessaloniki (AUTH), Greece in 2004, the MSc degree in Medical Informatics in 2008 from the Medical School, AUTH and the Ph.D. degree in Computer Networking from the Dept. of Informatics, AUTH in 2014. He is currently a postdoctoral research fellow at the Foundation Of Research and Technology, Hellas (FORTH).



Ageliki Tsioliariidou received the Diploma (2004) and the Ph.D degree (2010) in Electrical and Computer Engineering from the Democritus University of Thrace (DUTH), Greece. Her research in Computer Networks focuses on congestion control, fair allocation of network resources, as well as convergence potential and speed of routing protocols. She has contributed to a number of EU, ESA and National research projects. She is currently a postdoctoral fellow at the Interconnected Systems Laboratory, DUTH.